ELECTROCHEMICAL BEHAVIOR OF CARBON MATERIALS

Agustín E. Bolzán and Alejandro J. Arvia

Instituto de Investigaciones Fisicoquímicas Teóricas y Aplicadas (INIFTA), UNLP-CIC-CONICET, La Plata, Argentina

Contents

19.1 A BRIEF SUMMARY OF ELECTROCHEMICAL CONCEPTS

19.1.1 The Electrochemical Interface

Electrochemical reactions involve the transfer of electric charge across an interface consisting of an electrode (metal or semiconductor) in contact with an ionic conductor (electrolyte solution, molten salt, or solid electrolyte). The electrode material–ionic conductor interface exhibits a high electric capacitance. For instance, its value for a spherical gold surface in 1 M $NaClO_4$ aqueous solution is on the order of 10^{-6} F, in contrast with the capacitance of the same

spherical surface gold–vacuum interface that amounts only to about 10^{-13} F. This large difference is due to a spatial charge localized at the immediate vicinity of the metal in the electrochemical interface.

The electrochemical interface is considered as ideally polarizable when the application of any potential difference between both the phases produces no charge transfer across it. In this case, when an electrical potential is applied, a transient current (capacitive current) related to the electric charges on both sides of the interface can be measured. The reverse situation is the ideally nonpolarizable electrochemical interface. In this case, for any applied electric potential the charge transfer across the interface involves a transient capacitive current and a faradaic current that is exclusively related to an electrochemical reaction. Real electrochemical interfaces are intermediate between the two limiting polarization situations.

The region of the electrochemical interface comprising an electrolyte layer of a certain thickness in contact with the electrode surface in which the charge distribution differs from that in the bulk of the ionic conductor is known as the electrical double layer region. In this region, long- and short-range electrostatic forces determine both the structure of the electrochemical interface and in part the kinetics of faradaic processes. At the electrical double layer, the electric charge accumulated on the metal is equal to that in the ionic conducting phase. The sign of this charge is either positive or negative depending on the polarity of the applied electric potential.

The thermodynamics of the electrochemical interface is based on the Gibbs adsorption equation. For a plane electrode in contact with an ionic conductor, under equilibrium conditions, the Gibbs equation is [1]

$$d\gamma = -\sigma dT - \Gamma_e d\bar{\mu}_e - \sum_i \Gamma_i d\bar{\mu}_i - \sum_j \Gamma_j d\bar{\mu}_j - \sum_k \Gamma_k d\bar{\mu}_k - \sum_h \Gamma_h d\bar{\mu}_h \quad (19.1)$$

where γ is the surface tension, σ is the excess of entropy, T is the absolute temperature, Γ_x is the surface excess of component x, $x = e$, electron, $x = i$, ionic conducting species; $x = j$, $x = k$, and $x = h$ cations, anions, and neutral species, respectively; $\bar{\mu}_x$ is the electrochemical potential of x

$$\bar{\mu}_x = \mu_x + z_x F\phi \quad (19.2)$$

μ_x, z_x, and ϕ being the chemical potential of x, its electric charge and the inner phase potential (Galvani potential), respectively, and F is the Faraday constant. The chemical potential μ_x is given by

$$\mu_x = \mu_0 + RT \ln a_x \quad (19.3)$$

where a_x is the activity of component x, and μ_0 its chemical potential when $a_x = 1$.

Considering that $\Gamma_h = 0$ and $\Gamma_e = q_M$, at constant temperature (T), pressure (P), and solution composition, it results in

$$\left(\frac{\partial \gamma}{\partial \phi}\right)_{P,T,\mu} = -qM \tag{19.4}$$

Relationship (19.4), known as Lippmann equation, permits the evaluation of the excess of charge at the electrode surface from the electrocapillary curve $\gamma = \gamma(\phi)$. For interfaces relatively simple such as the mercury/1 M aqueous KCl interface, Eqn (19.4) results in a parabola with a maximum at $\partial \gamma / \partial \phi = 0$, i.e., for null charge at the electrode surface. This condition corresponds to the potential of zero charge (E_{pzc}) for the electrode in the electrolyte solution.

The second derivative of Eqn (19.4) represents the capacitance C

$$\left(\frac{\partial^2 \gamma}{\partial \phi^2}\right)_{P,T,\mu} = -\left(\frac{\partial q^M}{\partial \phi}\right)_{P,T,\mu} = -C \tag{19.5}$$

When $\gamma = \gamma(\phi)$ is a perfect parabolic function, it results that $d\gamma/d\phi$ is proportional to ϕ, and the electrochemical interface is characterized by a constant value of C.

For real systems, $\partial q^M / \partial \phi$ changes with ϕ, and therefore a differential capacitance (C_d) has to be defined

$$C_d = \left(\frac{dq^M}{dE}\right)_{P,T,\mu} \tag{19.6}$$

where E is the electric potential difference across the capacitance. Values of Γ_i and γ can be obtained by integration of the electrocapillary curve provided that the value of E_{pzc} is known.

19.1.2 Adsorption at Electrodes

In the absence of chemical or electrochemical processes, the adsorption of molecules, ions or both at the electrode surface becomes possible. This fact involves electrode-solvent, electrode-ionic species, and solvent-ionic species as the most relevant interactions and the possible contribution of lateral interactions. These interactions play an important role in the behavior of C vs E curves.

The adsorption of either ions or neutral molecules on the electrode surface depends on q_M, i.e., on the applied electric potential. Correspondingly, the electric field at the electrochemical interface is an additional free-energy contribution that either favors or restricts the adsorption of species on the electrode from the ionic conducting phase. A variety of adsorption isotherms has been proposed to account for the behavior of different electrochemical systems. Among them are the Langmuir, Frumkin, and Temkin isotherms [2]. Frumkin and Temkin isotherms, at variance with the Langmuir one, include effects such as adsorbate–adsorbate or adsorbate–surface interactions.
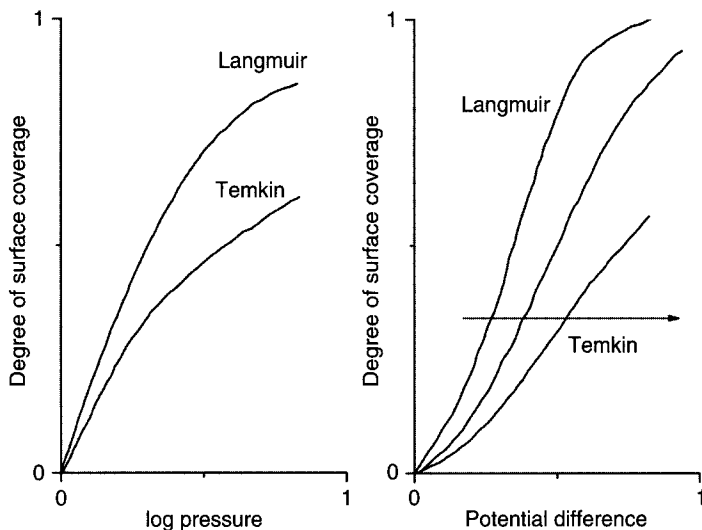
Figure 19.1 Comparison of chemical and electrochemical isotherms. The arrow indicates the shift of the curves as the lateral interactions term increases.

A comparison of the dependence of θ_i, the degree of surface coverage by species i, on either P (chemical adsorption) or E (electrochemical adsorption) is shown in Fig. 19.1.

At the electrochemical interface, adsorption of either charged or neutral molecules and charge transfer processes may occur simultaneously. Electroadsorption and electrodesorption processes play a key role in electrocatalytic reactions [2].

19.1.3 Relevant Kinetic Parameters

The rate of an electrochemical reaction involving reactant i, expressed as dN_i/dt, where N_i is the number of moles of i electrolyzed at time t, is proportional to the faradaic current (I) flowing across the cell. However, as the electrode process is a heterogeneous reaction, its rate is usually expressed as moles s cm^2

$$\frac{1}{A}\frac{dN_i}{dt} = \frac{j}{z_i F} \tag{19.7}$$

where A is the electrode area and j is the current density, i.e., $j = I/A$.

A basic problem in electrochemical kinetics is to determine the current (I) as a function of the applied potential (E), particularly under steady-state conditions. The departure of the electrode potential from the equilibrium value (E_{rev} = Nernst potential) is the electrode polarization that is measured by the overpotential (η)

$$\eta = E - E_{rev} \tag{19.8}$$

The overall current efficiency for the nth process is given by the ratio between the fraction of the number of coulombs (Q_n) involved in the nth process and the total charge (Q_T) passed across the cell

$$\rho_n = \frac{Q_n}{Q_T} \tag{19.9}$$

For a single electrochemical process $\rho = 1$.

Generally, the rate of the electrode process is influenced by the mass transport of reactants to and products from the electrode surface, the proper electron transfer process, and the chemical reactions preceding or following the electron transfer. Accordingly, the value of η may involve a concentration (mass transport), activation (electron transfer), and ohmic (ohmic resistance) polarization contribution.

Let us consider a simple redox reaction involving species O and R in the solution

$$O + ze^- \underset{k_f}{\overset{k_b}{\rightleftharpoons}} R \tag{19.10}$$

k_f and k_b being the rate constants for the forward (f, cathodic) and backward (b, anodic) reactions. The net current flowing through the electrochemical interface is the algebraic sum of the currents I_f and I_b of the partial reactions

$$I = I_f - I_b = zFA\left[k_f c_O\left(0, t\right) - k_b c_R\left(0, t\right)\right] \tag{19.11}$$

$c_O(0,t)$ and $c_R(0,t)$ being the concentration of O and R on the electrode surface at time t. The rate constants depend on the overpotential

$$k_f = k^0 \exp\left[-\frac{\alpha zF}{RT}\left(E = E^0\right)\right] \tag{19.12}$$

$$k_b = k^0 \exp\left[-\frac{(1-\alpha)zF}{RT}\left(E = E^0\right)\right] \tag{19.13}$$

k^0 being the standard rate constant, α the transfer coefficient assisting the reaction in the forward direction, and E^0 the standard potential of the redox reaction. The value of k^0 is related to the exchange current density (j_0) of the reaction at the reversible potential. Equations (19.12) and (19.13) are usually expressed as Tafel relationships. For the cathodic reaction, the Tafel equation is

$$\eta = a + b \ln j \tag{19.14}$$

with $a = RT/j_0\alpha$ and $b = -RT/\alpha F$. A similar Tafel equation can be written for the anodic reaction with $a = RT/j_0(1 - \alpha)$ and $b = RT/(1 - \alpha)F$.

Most electrochemical processes can be described by complex reaction mechanisms with a rate-determining step (rds). Besides, a stoichiometric number of the rds is defined as the number of times the rds has to occur for every complete act of the overall reaction.

From the temperature dependence of Eqs (19.12) and (19.13), the activation energy of the cathodic and anodic reactions at different values of η can be obtained.

19.2 THERMODYNAMIC DATA FOR CARBON ELECTRODES

Standard aqueous electrode potentials for reactions involving carbon have been calculated from the free energy of formation of carbon-containing compounds at different pH and temperature[3–6]. These data, displayed as potential–pH equilibrium diagrams, determine the domains of relative predominance of carbon as such or under a dissolved carbon-containing species such as methanol, aldehyde, acetic acid, carbonate, bicarbonate, or gaseous species such as methane, carbon dioxide, and carbon monoxide.

As an example, a scheme of a typical E/pH equilibrium diagram for graphite/water at 25°C is shown in Fig. 19.2. Lines (a) and (b) represent Nernst equation for the reduction (a) and oxidation (b) of water, respectively, under hydrogen and oxygen 1 atm pressure. Lines 1 and 2 delimit the regions for the equilibria between H_2CO_3, HCO_3^-, and CO_3^{2-} in aqueous solution free from
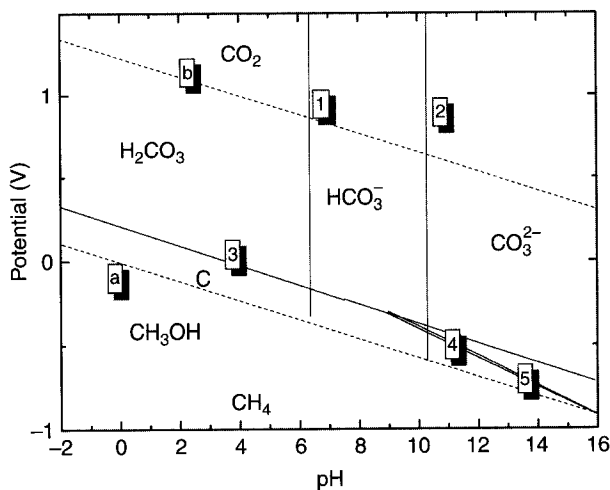

Figure 19.2 Potential–pH equilibrium diagram for the system C(graphite)–water at 25°C and for log(concentration) or log(partial pressure) equal to zero. (Reproduced from Ref. [3] with permission from Elsevier).

oxidizing agents. The domain above lines 3, 4, and 5 corresponds to solutions containing 1 M of dissolved carbon in the form of $H_2CO_3 + HCO_3^- + CO_3^{2-}$ (corrosion region). The domain below these lines refers to solutions saturated with solid carbon in equilibrium (immunity or stability region). Above line (b) CO_2 is the stable form of carbon. For $\log c = \log P_{CH_4} = \log P_{CO_2} = 0$, carbon in the form of graphite is thermodynamically stable only over a limited domain.

Thermodynamic data have also been calculated for carbon–oxygen reactions in fused salts [7, 8]. The oxidation of solid carbon principally yields carbon dioxide at low temperature and carbon monoxide at high temperature. In this case, at constant temperature, the CO/CO_2 concentration ratio at solid carbon depends on pressure. The carbon–oxygen electrode is used as reference to investigate cryolite–alumina melts at c. 1000°C [9] and molten slags at higher temperatures.

Thermodynamic data for other systems involving carbon and carbon-containing compounds are given in the original publications [3, 6, 10].

19.3 RELEVANT CHARACTERISTICS OF CARBON ELECTRODE MATERIALS

19.3.1 Types of Carbons Used in Electrochemistry

Carbon has been widely used since the times of Humphrey Davy (1778–1829), who used charcoal electrodes in some of his experimental work [11]. Carbon electrodes are extensively employed in a large number of electrochemical processes [12, 13], including electrochemical energy storage and energy conversion devices, halogen production, electrometallurgical processes in melts and aqueous solutions, water preparation and water decontamination systems, preparation of organic compounds by chemically modified electrodes, as well as inorganic electrosynthesis to generate peroxide, ozone, fluoride, chloro-alkali, and metals from fused salts [14, 15].

Carbon and graphite are often used as supports for electrocatalysts, but they also have an electrocatalytic function in electrode reactions such as oxygen reduction in alkaline electrolytes, chlorine alkali industry, and $SOCl_2$ reduction in lithium–thionyl chloride batteries.

Carbon electrodes are also employed in electroanalytical applications due to the very low residual current over a wide range of potentials that makes it possible to study electrochemical reactions even at the level of trace concentration. Among the different types of such electrodes, wax-impregnated graphite rods, carbon powder bound with an inert viscous liquid (carbon paste), glassy carbon, pyrolytic graphite and carbon fibers, and, more recently, nanotubes and fullerenes can be mentioned. Carbon fibers have radial, random, or anion distributions that lead to a different distribution of step and step–step interactions.

19.3.2 Structural Aspects

Carbon in the form of graphite behaves as a good metal. In the form of diamond it constitutes a wide-gap super hard semiconductor; with the intercalation of appropriate guest species it turns into a superconductor [16]; as a flexible polymer it reacts with hydrogen and other species. Carbon-based electrode materials show the entire range of dimensionalities (D) from fullerenes (0D quantum dots), to carbon nanotubes (1D quantum wires), to graphite (2D layered anisotropic material), and to diamond (3D wide gap semiconductor). Graphite represents the ground state for a system containing a large number of carbon atoms. Each small graphite sheet has a large energy per carbon atom at edge sites. In contrast, a small number of carbon atoms form closed shell configurations as in fullerenes and carbon nanotubes [17, 18].

The tunneling conductance between neighbor carbon nanotubes can be uniquely specified in terms of their individual chiral vectors and the pentagon and heptagon that must be introduced in the junction region. The conductance between two metallic nanotubes is found to be ballistic with some reflection effects occurring in the junction region. A metal semiconductor nanotube junction shows tunneling across the junction [19]. Results from scanning tunneling microscopy (STM) measurements indicate that one metallic nanotube 8.7 nm in diameter exhibits an ohmic behavior, whereas semiconducting tubules 4.0 and 1.7 nm in diameter show plateaus at zero current passing through null voltage. The slope of the current vs voltage plot provides a measure of the density of states. The current peak heights in these plots depend on the square root of the energy gap-dependent singularities in the 1D density of states. Semiconducting tubules show a linear dependence of their energy gap on the reciprocal tubule diameter [20].

The electronic and phonon dispersion relationships for pristine graphite have constituted the basis of models for other less well-ordered forms of graphite such as disordered graphite, graphite intercalation compounds, and ion-implanted graphite [16, 21]. The electrical resistance of carbon increases with oxygen chemisorption at the surface. Powdered carbon reactions with oxygen at 500–700°C result in a 4% oxygen content and in a 100-fold increase in the electrical resistance [22].

19.3.3 Surface Free Radical States

Electron paramagnetic resonance (EPR) is of considerable value for identifying paramagnetic surface groups and clarifying their role in electrochemical reactions. The variety of EPR characteristics of carbon and graphite reflects the diversity of structural and electronic properties of these materials that depend on crystalline size and perfection, impurities, preferred orientation, electrical resistivity, physical adsorption of gases, preparation procedure, and measuring techniques [23]. The surface of carbons is characterized by their capability for oxygen chemisorption at low temperatures. Well-defined crystalline graphite exhibit well-ordered stacks of carbon layers that are fairly unreactive toward

oxygen chemisorption, in contrast to more disordered structures such as carbon blacks yielding carbon–oxygen surface complexes.

Free radical states have an important role in the surface chemistry of carbons. They are formed as a result of thermal splitting of the C–H bonds to produce carbon rings. Unpaired electrons stabilize by occupying a molecular orbital in the π-bond system. The ratio between the electron density in the π-bond system and conduction electrons depends on temperature and on the treatment of the material.

Polyconjugated carbon structures that provide π-electrons usually involve three kinds of free σ-radicals: single radicals, side radicals, and σ-radicals without participation in the conjugated system. The electron capture by the broken σ-bonds is more favorable than that by the π-bond as the corresponding energy difference is about 403 J/mol. This fact leads to a variety of primary oxygen-containing surface states yielding the appearance of carbonylic, carboxylic, hydroxylic, and quinone groups at the edges of carbon layers. Hydrogen-containing groups are also formed, as demonstrated by surface analysis.

These surface states affect the chemical and electrochemical properties of carbon surface [24]. The amount of carboxylic and phenolic groups can be determined from the amount of nitrogen produced by their reaction with diazomethanes

$$R–COOH + CH_2N_2 \rightarrow R–COOCH_3 + N_2 \qquad (19.15)$$

$$ROH + CH_2N_2 \rightarrow R–OCH_3 + N_2 \qquad (19.16)$$
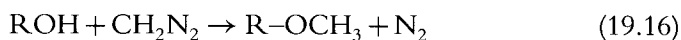
The distinction between these groups can be made by reaction of the carboxylic group with HCl [25]

$$R–COOCH_3 + HCL \rightarrow R–COCl + CH_3OH \qquad (19.17)$$

Quinone groups can be quantitatively determined from the amount of hydroquinones that is produced by reaction with $NaBH_4$ [25]. Lactones exhibit IR bands at $1760\,cm^{-1}$ because of the CO group of a lactone, and at $1600\,cm^{-1}$ because of the CO group hydrogen bonded to a phenolic OH. The band at $1600\,cm^{-1}$ disappears upon formation of the sodium salt.

The surface of carbons can be modified from hydrophobic to hydrophilic by means of oxidation processes. Consequently, carbons can exhibit selective adsorption properties depending on their oxygen content. For instance, commercial carbon blacks with a significant oxygen content selectively adsorb methanol from a methanol/benzene mixture, whereas one with much lower oxygen content exhibits selectivity for benzene.

19.3.4 Double-layer Properties

The capacitance–potential curves of the basal plane of highly ordered pyrolytic graphite (HOPG) (Fig. 19.3) show an anomalous low capacitance
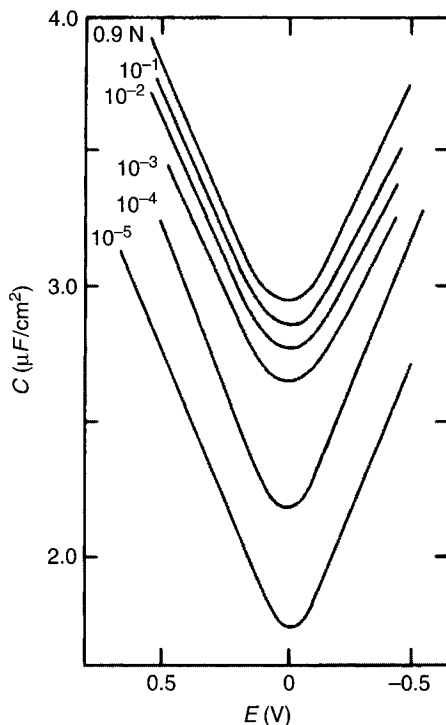
Figure 19.3 Capacitance–potential curves for HOPG in NaF solutions of pH of about 6 at 25°C; a.c. measurements at 20 Hz. (Reproduced from Ref. [26] with permission from Elsevier.)

value that is in the range 1.9–3.0 µF/cm^2, depending on the electrolyte solutions concentration [26]. It exhibits a negligible frequency dependence, both in acid and in base, and is nonsensitive to the presence of iodide in the solution. These facts indicate that the surface is free of functional groups to interact with the ions. The low capacitance value for the basal plane is related to a space charge caused by the semimetal characteristics of HOPG.

The capacitance–potential curve of graphite is essentially parabolic rather than hyperbolic, probably because of imperfections on the exposed basal plane giving rise to sites with degenerated surface electronic states. Thus, the capacitance calculated from slow scan voltammetry is about 29 µF/cm^2 at −0.2 V (vs normal hydrogen electrode (NHE)), a value considerably higher than that obtained from alternating current impedance measurements. This suggests that the much larger capacitance represents a portion of the surface with a micro-orientation that exposes other than the basal plane, or it might correspond to the possible existence of microfissures or microvoids. Exposed edge orientations have a much higher capacitance of about 60 µF/cm^2 that adds a large resistive component in series arising from the electrolyte resistance. Similar conclusions have been derived from glassy carbon [27]. Conversely, the voltammogram of HOPG in 0.5 M aqueous H_2SO_4 and 1 M aqueous NaOH at 25°C is relatively featureless

at least in the range 0–0.75 V (vs NHE), in agreement with the features of the capacitance/potential curves [28].

The potential distribution across the carbon–electrolyte solution interface in general will be changed by the surface functional groups. Correspondingly, the oxygen-containing groups may influence the potential of zero charge and the potential at the outer Helmholtz plane (OHP) of the electrical double layer [1]. Thus, even for the redox species that are not specifically adsorbed, their concentration at the OHP would be changed and this would also affect the kinetics of the reaction. Potentials of zero charge of various types of carbons in aqueous solutions are in the range 0.0–0.32 V (vs NHE) [6]

Black carbons form a homogeneous material series with graphitized black as the reference. For this series the chemical response ranges from Lewis base-like to Brnsted acid-like, while the work function varies appreciably through a minimum across a seven order of magnitude variation in the aqueous solution pH. The decreasing portion shows the lessening influence of the Lewis basic-like carbon basal plane electronic structure as acidic localized oxide functionalities are added to the carbon surface. The subsequent increase in the work function for pH < 6 is attributed to the accumulation of an outwardly pointing surface dipole layer with electric dipoles of 2.6 D associated with the stronger (carboxyl) acidic functionalities. The work function measurement has been made using the Kelvin–Zisman reciprocal capacitor technique that consists of determining the contact potential difference between the carbon black and a gold reference surface. Values of the work function are in the range 0.19–0.30 eV [29].

Capacitance measurements of carbon electrodes have also been made in molten halides, particularly chlorides [30–32], molten nitrates [33, 34], and in cryolite–alumina melts (graphite and glassy carbons). In cryolite–alumina melts, the double-layer capacitance of the basal plane of graphite, in the range 0.7–1.0 V (vs aluminum reference electrode) is about $20 \, \mu F/cm^2$ at 0.9 V, i.e., in a potential range where no appreciable flow of current has been observed. Data indicate that the capacitance is influenced by adsorbed species from the melt, possibly yielding intercalation compounds, and uncertainty in the true area of the electrode [34].

19.3.5 Roughness Factor

Carbon surfaces, except the HOPG basal plane, have some degree of roughness. The roughness factor (σ) can be defined as

$$\sigma = A_m/A_g \tag{19.18}$$

On the assumption that the surface roughness is on a distance scale which is large compared to the analyte molecules, A_m is the microscopic area that is relevant for adsorption or kinetic measurements. A_g is the geometric area determined either visually or by chronoamperometry on a scale where $\sqrt{D_i t}$ is much greater than any surface roughness. D_i is the diffusion coefficient of the reactant

i in the ionic conductor and t the electrolysis time. The value of $\sigma > 1$ refers to the entire microscopic area disregarding the amount or distribution of edge planes.

For the edge plane area (A_{edge})

$$A_{edge} = A_g \sigma f_e \tag{19.19}$$

f_e represents the fraction of edge planes on the surface, and depends strongly on the nature and preparation of the carbon surface.

The roughness of carbons is sensitive to the applied potential routine, as seen by sequential nanoscopic images of HOPG surfaces in aqueous solutions subjected to potential cycling of different duration [35] (Fig. 19.4). A stabilized carbon electrode topography merges after a prolonged potential cycling. These topographic changes can be described as time effects that depend on the type of carbon and ionic conductor, and the characteristics of the current or potential perturbation routines [20].

19.3.6 Fractality

The problem of transfer across a fractal surface has been considered in the electrochemical behavior of rough and porous carbon electrodes [36]. The fractal dimension can be determined from nitrogen gas adsorption data, from transmission electron microscopy (TEM), and nanoscopy image analysis.

Fractal electrodes exhibit a constant phase element (CPE) behavior in electrochemical impedance spectroscopy (EIS) [37]. The relationship between the CPE behavior of rough, irregular electrodes and fractality depends on the scale of irregularities, i.e., whether it is on the micrometer or centimeter scale. In real situations, however, both microscopic and macroscopic geometric effects probably occur simultaneously.

For imprinted mesoporous carbons, the overall fractal dimension, determined from gas adsorption data, indicate that these materials are composed of two groups of pores. The surface fractal dimension of the carbonization-induced pores surface and that of the silica-imprinted pores surface has been obtained from TEM image analysis [38].

19.3.7 Intercalation of Ions in Graphite

Intercalation constitutes an important case of inclusion phenomena in which the host lattice is characterized by a lamellar structure [39]. Graphite yields both anion and cation intercalation compounds and charge transfer processes are the driving forces for their formation.

Due to the action of an oxidizing agent electrons are drawn from the graphite lattice and anions beside neutral species are intercalated. These processes can be driven in a direct reversible electrochemical way, as has been demonstrated for carbon in concentrated sulfuric acid [39].

For a graphite electrode in concentrated acid solution, the formation of intercalation compounds occurs when the threshold potential for the intercalation
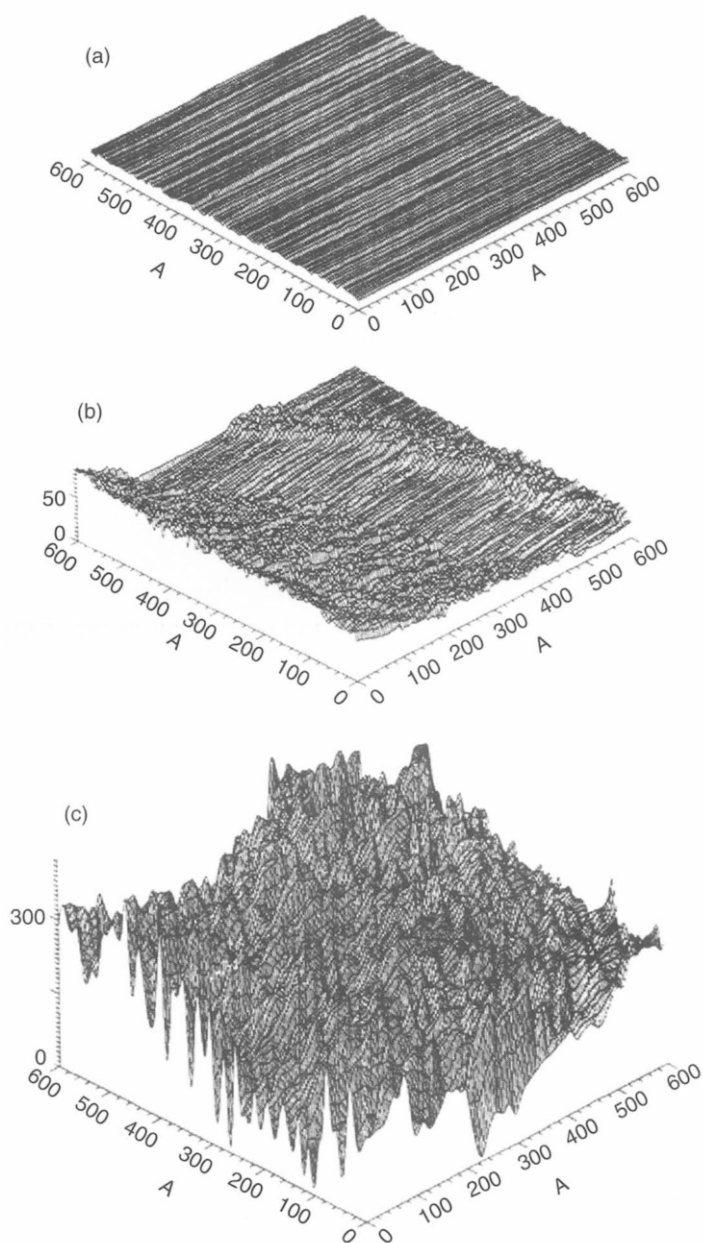
**Figure 19.4** Constant-current scanning tunneling microscopy images ($600 \times 600 \, nm^2$) of HOPG after anodic oxidation in $0.1 \, M \, H_2SO_2$ at $0.05 \, V$ vs Ag/Ag^+ electrode. (a) HOPG surface before electro-oxidation (blank); (b) HOPG surface after 20 potential cycles; (c) HOPG surface after further electro-oxidation cycles. (Reprinted with permission from Ref. [35]. © 1988 American Chemical Society.)

process is exceeded (intercalation overpotential). The first step of this process is the oxidation of graphite to form a macroradical cation

$$C_x \rightleftharpoons C_x^+ + e^- \tag{19.20}$$

the electron being removed from the highest filled level of graphite. This process resembles the anodic oxidation of organic hydrocarbons such as perylene yielding a radical cation. In both cases, the anion acts as the counterion required to balance the positive charge. The second step is the transfer of anions across the electrochemical interface

$$C_x^+ + A^- (solv)_n \rightleftharpoons (C_x^+ A^-)_i + n\text{solv} \tag{19.21}$$
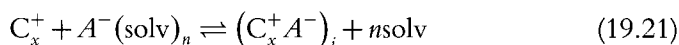
and correspondingly, the graphite lattice has to be expanded. For weakly solvated cations of low melting points, this process is highly reversible, as has been concluded from voltammetry and impedance measurements [39].

For carbon in concentrated sulfuric acid, the overall reaction can be represented as follows:

$$C + HSO_4^- + 2H_2SO_4 \rightleftharpoons [C_x (HSO_4) (2H_2SO_4)]_i + e^- \tag{19.22}$$
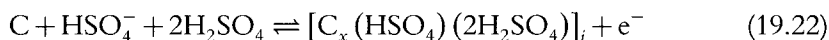
From reaction (19.22) intercalation compounds (i) with $x = 24$ have been obtained.

Alkaline metals, particularly rubidium, potassium, and cesium, intercalate graphite layers yielding compounds of the form C_8Me when a layer of alkaline metal atoms is formed between each pair of carbon planes [6].

19.4 CHEMICALLY MODIFIED ELECTRODES AND SUPRAMOLECULAR CONFIGURATIONS

The electrochemical and electrocatalytic properties of carbon electrodes can be modified changing their surface composition by anchoring foreign compounds. This can be accomplished by adsorption, by chemical reaction with a surface group, by specific chemical binding, and by adsorption immobilization on a sublayer of a polymer material [40]. Chemically modified electrodes constitute a part of supramolecular chemistry.

Typical examples of the adsorption procedure are the irreversible attachement of metal-N_4 complexes on HOPG and the adsorption of aromatic molecules for anchoring complex species.

Ion–N_4 complexes are adsorbed in a planar orientation on the HOPG surface and cobalt and iron tetrasulfate phtalocyanines are arranged sideways relative to the surface [41].

Complexes like $[Ru(NH_3)_5L]^{2+}$ with a large aromatic ligand such as 4-aminomethylpyridine or N-(4-picolinic)benzamide; $[(Rubipy)_2L]^{2+}\cdot2(PF_6^-)$; 1,5 diihydroxyanthraquinone, can be adsorbed on glassy carbon by evaporation from a nonaqueous solution [42].

For chemical attachment, the carbon surface is first activated by oxidation at 160°C in air or by oxygen plasma. Then, activated COOH carbon groups react with thionyl chloride yielding –COCl groups at the carbon surface. Subsequently, the active group (R) is attached via a reaction with amines leading to –CONHR. Thus, different functional groups (R) can be attached.

Covalent attachment of active molecules to graphite surfaces can be made via OH groups using cyanuric chloride, 2,4-dinitrophenylhydrazine or chlorosilanes as intermediate reagents [43].

The adsorption of polymers, poly(vinyl pyridine) or poly(acrylonitrile) either to coordinate metal atoms or to adsorb biopolymers has been used to prepare chemically modified electrodes for immobilization of enzymes either by physical or by chemical adsorption (carrier binding), cross-linking, and entrapping at lattice sites or in microcapsules [43]. A wide application of these types of electrodes has been made for electrochemical reactions of biological interest [44].

Chemically modified electrodes resulting from the attachment of quinones, phenantroline, dipyridyl complexes, and N_4 complexes, from the development of polymer-coated carbon materials, and from electrodes modified by enzymes have been specifically designed for the electrocatalytic reduction of molecular oxygen (OERR). Carbon materials with immobilized hydroquinone have also been utilized to accelerate the electrochemical oxidation of molecular hydrogen.

Modified carbon and graphite electrodes have been found adequate for producing a mixture of optically active isomers and stereoselective addition reactions such as the chlorination of anisole at an α-cyclodextrine-modified graphite electrode [45].

The kinetics of the electrochemical reactions at arrangements of chemically modified electrodes has been interpreted by a charge and mass transfer electrochemical mechanism. Charge transfer can be, in general, described by an electron jump and a molecular diffusion step. At electrodes modified by complexes, the rate of electron tunneling ($W(r)$) can be described by the equation

$$W(r) = V'\exp\left(-r/A'\right) \tag{19.23}$$

r being the distance covered by the electron, V' is a constant, and A' depends on the geometry of the potential energy barrier. Accordingly, the transfer efficiency should depend on the distance from the active center to the electrode plane. For $r < r_{crit}$, $W(r)$ should be greater than the rate of the reaction at the active center. For $r > r_{crit}$, the reverse situation occurs.

The influence of r on the rate of the OERR has been studied on laccase-modified carbon electrodes [46]. In this case, r was varied by a monolayer of adsorbed lipid that had either planar (cholesterol) or vertical (lecithin) orientation on the electrode surface. In this case, a sharp decrease in the rate of OERR was found within a narrow range of r, which is determined by $r_{crit} \approx 2\,nm$.

The diffusion step becomes important for polymer-modified electrodes. Thus, the apparent diffusion coefficient depends on the concentration of redox groups because the acceleration of the electron exchange decreases with the ion distance. These conclusions were drawn from a series of polyvalent ions anchored electrochemically to poly(4-vinyl pyridine) on graphite [47].

Electronic conductivity is favored by electron transfer through the polymer delocalized band structure, via redox conductivity by site–site hopping. Redox conductivity occurs at electron energies centered around the formal equilibrium potential for the redox polymers.

19.5 ELECTROCHEMICAL KINETICS ON CARBON ELECTRODES IN AQUEOUS SOLUTIONS

19.5.1 Direct Electrode Processes

Although carbon electrodes are frequently used for electroanalytical studies of oxidizable compounds, many of them exhibit heterogeneous charge transfer rates that are very low at carbon electrodes, as concluded from their corresponding ill-defined voltammograms [48]. Thus, the surface properties of carbon electrodes can have remarkable effects on the voltammetric response of these direct electrode reactions.

One typical example of this behavior is the voltammogram of the ferro/ferricyanide couple (test reaction) that at carbon electrodes is less reversible than at noble metal electrodes. The kinetics of the test reaction in 1 M aqueous KCl was used as the reference to compare its electrochemical behavior on different carbon electrodes [20]. This electrochemical reaction occurs via an outer sphere mechanism and its rate depends on the electrolyte composition and can be increased by appropriate treatment of carbon electrodes, for instance, by application of a high current potential routine to electrodes of carbon fibers. Similar results have been obtained with glassy carbon surfaces that had been pretreated at $500°C$ under reduced pressure. An alternative activation method is based on careful electrode surface polishing [6].

The kinetics of the test redox reaction on the cleavage HOPG surface is almost under pure diffusion control, whereas on the edge surface, where ion-specific adsorption is favored, it is under combined kinetic and diffusion control. Accordingly, surface heterogeneity is a new variable in the kinetics of electron transfer processes at carbon surfaces, as the surface energy of sites at each domain (plane, edges, kinks, etc.) is different. Let us assume the existence of two surface domains ($1 = $basal and $2 = $edge) for graphite with specific rate constants for the test reaction (k_1^0 and k_2^0) and consider that the 1-1 and 2-2 domain distances are R_{11} and R_{22}, respectively. The value of these distances relative to $\sqrt{Dt}$ may have a significant effect on the voltammetry that depends on whether $R_{11}, R_{22} \ll \sqrt{Dt}$, $R_{11} < \sqrt{Dt} < R_{22}$, and $R_{11}, R_{22} \gg \sqrt{Dt}$. The value

of $k_2^0 = 0.10\,\mathrm{cm/s}$ is about 25 times greater than $k_1^0 = 0.004\,\mathrm{cm/s}$, in agreement with the difference in reactivity between the basal plane of graphite and the edge sites. The remarkable anisotropy of k^0 coincides with that of C, E_{pzc} and the work function (Section 19.3.4).

Carbon composites have been developed as alternative materials for carbon paste electrodes because of the limited utility of the latter in most organic solvents. These composites include polyethylene/carbon black [49], Kel-F/graphite [50], carbon black immobilized in cross-linked polyethylene [51], and epoxy/graphite [52]. A collection of k^0 for these materials is available [20]. Thus, for platinum $k^0 = 0.24\,\mathrm{cm/s}$, for pyrolytic graphites $0.002 < k^0 < 0.007\,\mathrm{cm/s}$, and for graphite carbons $0.005 < k^0 < 0.14\,\mathrm{cm/s}$.

Simple redox solutes, ferrocene, N, N, N, N-tetramethyl-1,4-phenylenediamine, decamethylferrocene, bis(i-propylcyclopentadienyl) iron(II), $[\mathrm{Ru(phen)_3}]$ $(\mathrm{ClO_4})_2$, $[\mathrm{Fe(bpy)_3}](\mathrm{ClO_4})_2$, $[\mathrm{Co(bpy)_3}](\mathrm{ClO_4})_2$, and iodine have been studied at electrodes modified with polymeric fullerene films. Fullerene-modified electrodes were prepared by electropolymerization of C_{60} initiated by traces of dioxygen or by simultaneous electroreduction of fullerene and Pd(II) acetate trimer. For the former films, the electrochemical activity decreases upon potential cycling. The electrochemical activity of the film is stabilized by the redox solute added to the electropolimerization stage due to the catalytic oxidation of the fullerene film by the oxidized form of the redox system. Similarly, positively charged species can also be incorporated into the structure of the film. The reversible behavior of redox solutes decreases with the increase in the thickness of the Pd/C_{60} film. This film also incorporates ferricinium ion, N, N, N, N-tetramethyl-1,4-phenylenediamine cation, decamethylferricinium ion, and to a smaller degree $[\mathrm{Co(bpy)_3}]^{n+}$ [53].

Microcrystals of fullerene-C_{60} on glassy carbon mediate the oxidation of cysteine in the presence of aqueous potassium-containing electrolytes. The potential for the oxidation of cysteine is lowered by approximately $100\,\mathrm{mV}$ and current is enhanced significantly as compared to bare glassy carbon electrodes. Additional mediation occurs when the potential range of C_{60}/C_{60}^{n-} redox couples are covered. The electrochemical response is sensitive to pH, temperature, and C_{60} dosage. Excellent analytical and/or recovery data are obtained with vitamin pill (alcovite), cassamino acid (hydrolyzed casein), and for a range of beverages [54].

19.5.2 Oxygen Electroreduction on Carbon Electrodes

The reversible potential of the water decomposition reaction is $1.23\,\mathrm{V}$ at $25°\mathrm{C}$. The overpotential for OERR in aqueous alkaline solutions

$$O_2 + H_2O + 4e^- \rightarrow 4OH^- \tag{19.24}$$
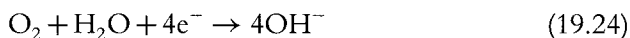
is 0.3–$0.4\,\mathrm{V}$ at 60–$80°\mathrm{C}$, and in acid solutions

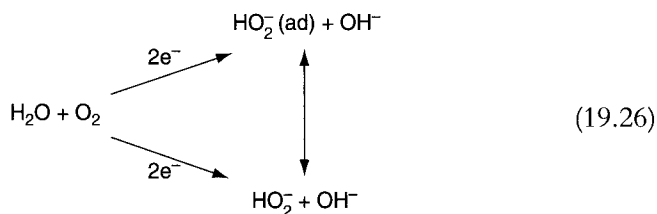$$O_2 + 4H^+ + 4e^- \rightarrow 4OH^- \tag{19.25}$$
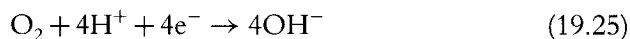
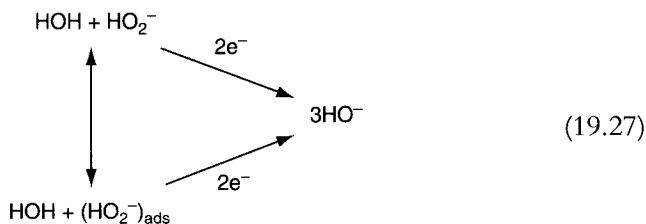it is 0.4–$0.5\,\mathrm{V}$ at c. $190°\mathrm{C}$

The oxygen electrode polarization is a measure of the degree of irreversibility of the electrochemical reaction. To find an effective electrocatalyst for reactions (19.24) and (19.25) is of a great interest because of their technical relevance in water electrolysis, fuel cells, metal corrosion in aqueous environments, biological processes, etc.

The OERR is usually considered to proceed via two reaction pathways, namely, the peroxide and the direct four-electron pathways.
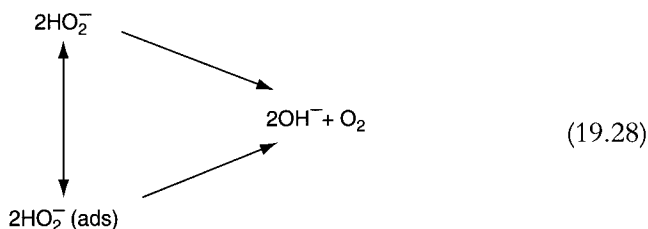
The scheme of the peroxide pathway is

$$
\begin{array}{ccc}
 & & HO_2^- \, (ad) + OH^- \\
 & \nearrow^{2e^-} & \uparrow \\
H_2O + O_2 & & \\
 & \searrow_{2e^-} & \downarrow \\
 & & HO_2^- + OH^-
\end{array}
\qquad (19.26)
$$

where (ad) stands for peroxide adsorbed species on carbon. The peroxide species are either electroreduced further to OH^-

$$
\begin{array}{ccc}
HOH + HO_2^- & & \\
\uparrow & \searrow^{2e^-} & \\
 & & 3HO^- \\
\downarrow & \nearrow & \\
HOH + (HO_2^-)_{ads} & _{2e^-} &
\end{array}
\qquad (19.27)
$$

or catalytically decomposed to OH^- and O_2

$$
\begin{array}{ccc}
2HO_2^- & \searrow & \\
\uparrow & & 2OH^- + O_2 \\
\downarrow & \nearrow & \\
2HO_2^- \, (ads) & &
\end{array}
\qquad (19.28)
$$

The overall reaction is the four-electron electroreduction of molecular oxygen. The oxygen resulting from reaction (19.28) is recycled via reaction (19.26).

The direct four-electron pathway involves no hydrogen peroxide formation in the solution. This fact, however, does not preclude the participation of an adsorbed peroxide intermediate in the course of the reaction. The distinction between both reaction pathways is usually investigated by the rotating ring-disc electrode technique [55]. From the rotation speed and potential dependence of the disc electrode to ring electrode current ratio, it is possible to determine the relative contribution of each reaction pathway to the overall reaction [56].

19.5.2.1 OERR kinetics in alkaline solutions

The kinetics of the OERR on carbon [27] and graphite [27] in alkaline solution has been explained in terms of the dominant contribution of the peroxide reaction pathway. On the other hand, the direct four-electron pathway predominates on graphite electrodes modified by adsorbed tetrasulfonated phtalocyanine [57] and attached face-to-face di-cobalt–porphyrin complexes [58]. In principle, when both pathways operate simultaneously on a given surface, the kinetics is referred to as involving a parallel mechanism [59].

In alkaline solutions porous carbon electrodes are effective catalysts for the OERR. In this case, the exchange current density of reaction (19.26) for both carbon and graphite in $1\,M$ KOH $+\ 10^{-3}\,M$ peroxide concentration [59] is in the range $10^{-4} < j_0 < 10^{-3}\,A/cm^2$ (true area). For porous carbon electrodes (10^4–$10^5\,cm^2$ true area per cm^2 superficial area) large values of j_0 indicate a small activation polarization for the OERR. The predominant process occurs then via the peroxide pathway.

In general, the presence of impurities determines the extent of the rate of desorption of adsorbed peroxide, although the catalytic peroxide elimination effect decreases during the electrode operation. For porous structured carbons this effect can be due to the buildup of a substantial amount of peroxide in the solution within pores. Furthermore, the high peroxide concentration contributes to increasing the O_2^- radical ion and OH radical concentration within the pores via the following equilibrium:

$$HO_2^- + O_2 + OH^- \rightleftharpoons 2O_2^- + H_2O \qquad (19.29)$$
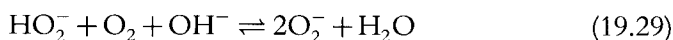
the equilibrium constant of reaction (19.29) being $K \approx 10^{-7.5}$ at 25°C [60].

Radicals such as O_2^- and OH, which are produced as intermediates in the homogeneous peroxide decomposition, may favor the attack of carbon via oxidation. This fact is accompanied by a change in hydrophobicity and porous clogging by gel formation, particularly because of sodium peroxide.

Suppression of HO_2^- concentration in porous carbon electrodes is usually accomplished by the dispersion in carbon of specific catalysts such as silver, MnO_2, and Ni–Co spinels.

For very active catalysts such as platinum supported on carbon, the direct four-electron and the peroxide-producing reaction occur in parallel, the first on the catalyst, and the latter on carbon surface domains. Accordingly, it is possible to diminish the peroxide activity to the equilibrium value of reaction (19.29). In this case, the electrode potential would approach the equilibrium value for the overall four-electron electroreduction reaction (19.24).
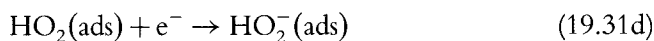
The stationary cathodic current–potential polarization curve of the OERR on pyrolytic graphite exhibits the Tafel slope $-0.120\,V$ per decade^{-1} at 25°C, and the stoichiometric number is 2 for the O_2 to OH_2^- electroreduction reaction. For glassy carbon, the Tafel slope is $-0.060\,V$ per decade^{-1}, and the corresponding stoichiometric number is 1, as expected for reaction (19.26) [28]. The OERR is first order in O_2 and zero order in OH^- for both carbons.

For graphite the following mechanism for the OERR has been proposed [27]:

$$O_2 \rightarrow O_2(ads) \qquad (19.30a)$$

$$O_2(ads) + e^- \rightarrow O_2^- \qquad (19.30b)$$

$$2O_2^-(ads) + HOH \rightarrow O_2 + HO_2^- + OH^- \qquad (19.30c)$$

with step (19.30b) being rate determining in the Tafel range of the polarization curve. Reaction (19.30c) is a complex process involving several steps.

For glassy carbon, the mechanism of the OERR [28] starts with reaction (19.30a) followed by

$$O_2(ad) + e^- \rightarrow [O_2(ads)]^- \qquad (19.31a)$$

$$O_2(ads)^- \rightarrow \{O_2(ads)\}^- \qquad (19.31b)$$

$$\{O_2(ads)\}^- + HOH \rightarrow HO_2(ads) + OH^- \qquad (19.31c)$$

$$HO_2(ads) + e^- \rightarrow HO_2^-(ads) \qquad (19.31d)$$

$$HO_2^-(ads) \rightarrow HO_2^- \qquad (19.31e)$$
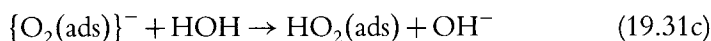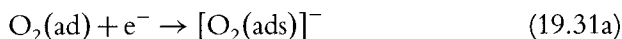
step (19.31c) being rate determining. $[O_2(ads)]$ and $\{O_2(ads)\}$ indicate different adsorbate structures.

For Teflon-bonded gas-fed electrodes prepared from carbons that have little peroxide-decomposing activity, the OERR at the highest current densities appears to be limited by converging characteristics related to carbon itself, its electrocatalytic activity for oxygen reduction to peroxide and peroxide decomposition, the gas mass transport, and the electronic conductivity.

To advance in the understanding of the OERR mechanism on carbon and graphite, more information at the molecular level of surface functional groups at these cathodes in air is still required.

19.5.2.2 OERR in acid solutions

In acid solution the OERR proceeds mainly via the formation of H_2O_2 on porous carbon electrodes. This is also supported by experiments with ^{18}O isotope that showed a lack of O–O bond break during the OERR. In acid media, the OERR appear to be independent of pH and the Tafel slope is close to $-0.120\,V$ per decade[1], the transfer of a first electron to an adsorbed oxygen molecule being the rds.

$$O_2(ad) + e^- \rightarrow O_2^-(ad) \qquad (19.32)$$

The reaction is first order with respect to molecular oxygen.

The efficiency of the OERR is increased considerably when mesometal and nanoparticles (Pd, Au) on carbon surfaces are used as electrocatalysts [61]. This electrocatalytic enhancement is related to the geometry of these metal islands

and it appears that the most active domains are located at edges of islands in contact with the HOPG surface [62]. This is consistent with the fact that gold nanoparticles electrochemically formed on graphite are preferentially deposited on the upper plane of step edges due to the nonuniform electron density that results from relaxation of the graphite lattice near steps [63].

19.5.3 Oxygen Reduction on Macrocyclic Transition Metal Complexes on Graphite and Carbon Surfaces

In contrast to the interaction of O_2 with graphite and carbon surfaces, the electrodes modified by transition metal complexes provide the possibility of extending the type of interactions derived from inorganic chemistry to the electrochemical system. A typical example is the face-to-face anchorage of porphyrins as catalysts on carbon electrodes for the OERR [58, 60, 64]. For cobalt porphyrin on graphite, when the Co–Co distance is about 0.4 nm, which makes the formation of an O–O bridge between Co centers possible, the presence of the Co porphyrin catalyzes the four-electron reaction in acid solutions, whereas for smaller Co–Co distances, the peroxide pathway is catalyzed. These behaviors have been related to the *cis* and *trans* surface complex configurations that assist the four-electron reaction and the peroxide pathway, respectively. Similar electrocatalysis for the OERR has been found in alkaline solutions when the macrocycles are adsorbed on graphite [28].

The thin layer of transition metal macrocycles attached to carbon generally lack long-term stability in concentrated acid and alkaline solutions. This drawback can be overcome by thermal treatment at 450–900°C for cobalt tetramethoxy phenyl porphyrin (Co-TMPP) [65]. Under these conditions, the Co-TMPP is substantially degraded to cobaltous oxide. Pyrolyzed layers involve high-area carbonaceous materials with a significant surface nitrogen and the transition metals as small oxide and metallic particles dispersed on the high-area substrate. These layers catalyze peroxide elimination in alkaline solutions.

The catalytic current for the OERR in aqueous solutions at glassy carbon electrodes modified by the physical adsorption of 1,2-dihydroxyanthraquinone is significantly increased under insonization because of the increase in mass transport [66].

19.5.4 Oxygen, Hydrogen, and Chlorine Electrode Reactions

Hydrogen, oxygen, and chlorine overpotential measurements on the basal and edge planes of stress-annealed graphite are complicated by intercalation and oxidative attack of the surface. Both hydrogen and oxygen overpotential are quite high on most graphite and carbon surfaces, probably in part because of the existence of functional groups. The interaction of adsorbed groups, both directly or through electronic substrate effects, would produce broad voltammetric peaks that reflect in large Temkin terms in the adsorption isotherm. This fact makes the voltammogram interpretation difficult.

19.5.4.1 Hydrogen evolution on carbon and graphite

Carbons exhibit a low electrocatalytic activity for the hydrogen electrode reaction (HER). Structural characteristics have significant electrocatalytic effects on the HER as j_0 changes from 2×10^{-9} to $2.5 \times 10^{-8}\,A/cm^{-2}$ on going from the basal plane to the side face of pyrolytic graphite. On glassy carbon, the HER overpotential decreases as the pretreatment temperature is increased. This thermal treatment leads to structural and chemical transformations from carbonization, precrystallization, and to graphitization.

Kinetic parameters for the HER on different carbon and graphite electrodes show that depending on the type of electrode and acid solution j_0 varies between 2×10^{-7} and $2 \times 10^{-13}\,A/cm^2$ and the cathodic Tafel slope is usually close to $-0.120\,V$ per decade, although some unexpected higher values have also been recorded. The reaction order with respect to the hydrogen ion concentration is 1, but unexpected values of 0 and 2 have also been reported [6]. The rds is usually the initial discharge step and the surface coverage of hydrogen atoms is low.

Electrochemical reductions of fullerene films in the presence of Brnsted acids yield hydrogenated fullerenes H_nC_{60}, where n depends on the acid, its concentration, and on the electrode potential. Hydrogenated fullerene films behave as semiconductors with increased photoefficiency [67].

19.5.4.2 Oxygen evolution on carbon and graphite

The rate of the oxygen evolution reaction (OER) on pyrolytic graphite is higher than that for glassy carbon. For both the carbon electrodes, the temperature pretreatment has no influence on the current measured at constant potential.

Carbon dioxide is the main reaction product for $E < 1.1\,V$ (vs reversible hydrogen electrode (RHE)) on pyrolytic graphite. For a pH between 1 and 9, the Tafel slope changes from 0.150 to 0.240 V per decade, depending on the solution composition and electrode preparation.

The anodization of both glassy carbon and HOPG in aprotic solutions (DMSO, ACN) is characterized by a reversible one-electron O_2 to O_2^- reaction.

Kinetic data of the oxygen electrode on carbon materials have been compiled in Ref. [68].

19.5.4.3 Chlorine electrode

In aqueous solutions, the equilibrium potential for the reaction

$$2Cl^- \rightleftharpoons Cl_2 + 2e^- \tag{19.33}$$

is $1.359\,V$ vs NHE at $25°C$ [3]. This figure is approached for smooth pyrolytic graphite in aqueous NaCl ($a = 1$) under chlorine saturation ($P_{Cl_2} = 1$) to attain $1.320\,V$ [6]. Therefore, carbons are useful for applications in the chlorine evolution reaction as both, the carbon oxidation reaction and the OER exhibit larger overpotentials.

The kinetics and mechanism of the chlorine evolution reaction in aqueous solutions have been studied on smooth, porous, and impregnated graphite [68, 69]. The Tafel slope depends also on the nature and history of carbons. For HOPG and glassy carbon, the anodic Tafel slope is about 0.060 and 0.120 V per decade at 25°C, respectively, whereas for a graphite electrode consisting of a section parallel to the c-axis, three regions in the polarization curve with anodic Tafel slopes from 0.060 to 0.160 V per decade have been observed.

For reaction (19.33), current flow for the porous electrodes is under ohmic regime. Specifically adsorbed anions hinder chlorine evolution, in contrast to cations such as Fe^{3+} that probably produce a change in the potential distribution at the electrical double layer.

The residual gas evolution at graphite, after switching the anodic current off, decays by desorption via self-discharge.

$$graphite(Cl)_{ad} + e^- \rightleftharpoons Cl^- \qquad (19.34)$$

$$Cl^- + graphite(Cl)_{ad} \rightleftharpoons Cl_2 + e^- \qquad (19.35)$$
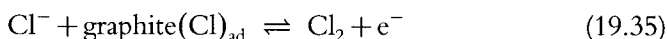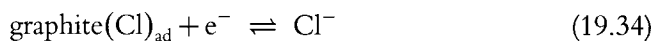
The rate of diffusion of atomic chlorine is determined by an equilibrium between diffusion of adsorbed chlorine from graphite outward (Eqn. (19.34)) and the formation of molecular chlorine (Eqn. (19.35)). As the surface concentration of chlorine diminishes, it is replenished by diffusion, a process that gradually becomes rate determining.

The kinetics of molecular chlorine evolution follows a first-order law with respect to chlorine, and zero order with respect to chloride ion concentration. The chlorine impregnation of carbon electrodes results in lamellar compounds such as C_8Cl [6].

The cathodic Tafel slope corresponding to reaction (19.33) in the reverse direction is close to -0.120 V per decade at 25°C. For both cathodic and anodic reactions, the interfacial capacity results in 30–$35\ \mu F\ cm^2$. This figure is consistent with a low surface coverage by chlorine atoms.
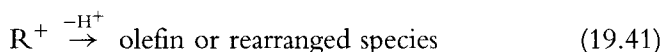
Kinetic parameters for the chlorine evolution reaction on carbon electrodes are assembled in Ref. [6].

19.6 ORGANIC ELECTROCHEMISTRY AT CARBON ELECTRODES

Carbon, graphite, vitreous carbon, carbon felt, carbon fibers and cloth, as well as reticulated carbons, are of common use either as anodes or cathodes for the electrochemical synthesis of organic compounds.

A typical example is the Kolbe electrosynthesis in which a carboxylate salt is electrochemically discharged at vitreous carbon anodes, in both aqueous and nonaqueous media, yielding a hydrocarbon with high efficiency and carbon dioxide.

At ordinary graphite electrodes in aqueous solutions, the reaction products are those derived from the formation of carbonium ion intermediates,

$$RCO_2^- \rightarrow R + CO_2 + e^- \tag{19.36}$$

$$2R \rightarrow R - R \tag{19.37}$$

$$R \rightarrow R^+ + e^- \tag{19.38}$$

$$R^+ \xrightarrow{H_2O} ROH + H^+ \tag{19.39}$$

$$R^+ \xrightarrow{RCO_2^-} RCO_2R \tag{19.40}$$

$$R^+ \xrightarrow{-H^+} \text{olefin or rearranged species} \tag{19.41}$$

The difference in the yields of products appears to be a carbon surface area effect that acts as product-determining characteristics.

For an extensive description of this matter, see Ref. [15].

19.7 REACTIONS ON BIOLOGICAL ACTIVE ELECTRODES

Electrochemical reactions of a large number of biological active compounds such as aminoacids, proteins, catecholamines, alkaloids, purines and their nucleosides, NAD, FAD, FMN, and nucleic acids have been investigated on HOPG, paste electrode, graphite, glassy carbon, carbon fibers, and fullerenes [68]. In this case, the ability of the anchored compound to remain stable by repetitive potential cycling between its different oxidation states is essential to successfully design a supramolecular electrode for this particular type of electrocatalytic reactions.

One example of this type of electrodes is a gold electrode covered by a self-assembled monolayer of gluthation and covalently bound fullerene [70], that has been proposed for the consecutive electro-oxidation of nicotinamide adenine dinucleotide (NADH) to NAD^+.

A first high power density of about $100 \, \mu W/cm^2$ miniature biofuel cell uses supramolecular modified carbon fiber electrodes operating in aqueous solution at pH 5 and room temperature. The electrocatalytic film at the anode catalyses the electro-oxidation of glucose to gluconolactone, and at the cathode catalyses the electroreduction of oxygen to water. The supramolecular ensemble involves Os^{2+}/Os^{3+} centers and enzymes that are immobilized in the electron-conducting redox-polymer films. The film of the anode consists of a cross-linked electrostatic adduct of glucose oxidase, and at 0.1 V (vs Ag/AgCl) a redox potential electron-conducting redox polymer, which electrically connects the glucose oxidase redox centres to one fibre. The film of the cathode consists of laccase and a 0.55 V

(vs Ag/AgCl) electron-conducting redox polymer, electrically connecting the laccase redox centres to the second fiber [71].

A miniature biofuel cell operating at 37°C in a glucose-containing aerated physiological buffer consists of two electrocatalyst-coated carbon fibers. Glucose is electro-oxidized to gluconolactone on the anode fibers and dissolved oxygen is electroreduced to water on the cathode fiber. The power output of the cell operating at 0.52 V is $1.9\,\mu W$, i.e., a power density of $4.3\,\mu W/mm^2$ [72].

These advances would increase the probability of achieving technical devices such as sensors, reactors, and energy storage and energy conversion devices, resulting from engineering and design approaches converging to the efficiency found in natural systems.

19.8 CORROSION PROCESSES

The degree of carbon corrosion depends on the type of carbon, the electrode potential, the temperature, and the carbon pretreatments that affect its surface structure [73].

Corrosion reactions occur at distinct domains of the carbon surface with different rates. The main surface domains are the plane boundaries or defects, outer interplanar areas, and intercalation areas between the planes. The stronger the edge attack, the greater the amorphous domains of carbons. Intercalation between the planes becomes more important with HOPG provided that some edges are exposed to the environment. The corrosion process changes with pH [74]. Nonbasal dislocations play an important role in the oxidation of graphite carbons.

In hot 96% phosphoric acid at 135–160°C different carbons exhibit similar corrosion behavior as a function of time [75, 76]. At constant potential, the corrosion current that was initially relatively large decreases rapidly with time. The principal corrosion reaction is

$$C + H_2O \rightarrow CO_2 + 2H^+ + 4e^- \tag{19.42}$$
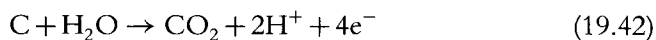
Different surface oxides are formed as intermediate oxidation products in reaction (19.42). Both the formation of surface oxides and the evolution of carbon dioxide decrease with time. But as the surface coverage by oxide increases, carbon dioxide formation prevails and proceeds via surface oxides at preferred sites. Corrosion rates of carbons appear to be independent of water content and carbon dioxide partial pressure.

In acid electrolytes, the Tafel slope for the carbon corrosion reaction appears to be indicative of the degree of disorder on the carbon surface. The larger the Tafel slope, the greater the degree of disorder. The influence of heat treatment on the corrosion rate depends on the structure of the parent carbon, particularly on the lattice parameters. Thus, in hot phosphoric acid at cathodic potentials, as

used in the phosphoric acid fuel cell technology at 150–200°C, samples of heat-treated Vulcan XC-72R after boron doping and heat treatment at 1000–2000°C show an enhanced resistance to corrosion. Changes in Brunauer, Emmit, Teller (BET) surface areas, lattice parameters, and electrochemical behavior converge to show that the addition of boron results in an additional graphitization to that achieved by the heat treatment itself. Boron acts as an electron acceptor and can enter the graphite lattice by substituting carbon atoms at trigonal sites that would provide traps for metal clustering.

The corrosion of carbon in alkaline solutions is of interest for alkaline batteries. For acetylene black electrodes at 0.45–0.60 V (vs Hg/HgO) in concentrated aqueous KOH, carbon dissolution to carbonate ion, gasification of carbon to carbon monoxide, and oxygen evolution are the main anodic processes, although the potential and temperature dependence of these processes is different. Correspondingly, for $E < 0.50$ V and $T < 50$°C, carbon dissolution is the primary process; for $0.50 < E < 0.60$ V and $T > 50$°C, carbon dissolution and oxygen evolution occur at comparable rates; for $E > 0.60$ V and $T > 60$°C, oxygen evolution and carbon gasification are the dominant processes. The current efficiency of these processes also depends on whether a catalyst such as cobalt oxide has been added to the carbon electrode, although the major effect is produced on the OER.

19.9 CARBON ELECTRODES IN MOLTEN SALTS

Carbon electrodes are crucial for a number of important processes in molten salt electrometallurgy. A long list of commonly used metals, such as aluminum, sodium, potassium, calcium, and magnesium are produced by these processes [77, 78].

19.9.1 Cryolite-Al_2O_3 Melts

Carbon anodes are used in the electrolysis of cryolite–alumina mixture to produce aluminum. The overall reaction in the electrochemical cell is

$$Al_2O_3 + 2C \rightarrow 2Al + CO + CO_2 \qquad (19.43)$$
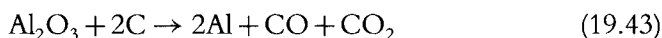
in which the anode is partially oxidized to CO and CO_2. The overall anodic reaction is

$$2O^{2-} + C \rightleftharpoons CO_2 + 4e^- \qquad (19.44)$$

However, considering reaction (19.43), reaction (19.44) has been interpreted by a complex reaction pathway that includes the formation of a C(O) surface intermediate as primary process
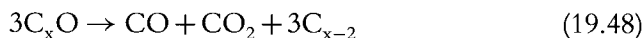
$$C + O^{2-} \rightarrow C(O) + 2e^- \qquad (19.45)$$

followed by a secondary chemical process yielding carbon oxides

$$C(O) \rightarrow \text{carbon oxides} \tag{19.46}$$

Another interpretation considers the formation of a nonstoichiometric surface oxide as primary process

$$xC + O^{2-} \rightarrow C_xO + 2e^- \tag{19.47}$$

that subsequently decomposes into CO and CO_2

$$3C_xO \rightarrow CO + CO_2 + 3C_{x-2} \tag{19.48}$$

The complex mechanism of reaction (19.44) is probably controlled by diffusion and the rate of the heterogeneous chemical reactions.

For various carbon electrodes in cryolite melts saturated with alumina at 1010°C, values of $0.0048 < j_0 < 0.24 \, A/cm^2$ have been reported [79].

The overpotential of the anodic reaction increases when the concentration of alumina in the melt decreases, and the wettability of the electrode by the melt decreases because of the accumulation of C(O), CO, and CO_2 species, leading to the dangerous anodic effect. Intercalation compounds such as $(CF)_n$, $(C_2F)_n$, and $C_xF(AlF_3)_y$ are also formed. Compounds having a covalent bond are unique in their low surface energy. The noncovalent intercalation compound results in a conductor better than the original carbon. These findings provided new methods for water proofing the carbon surface and for new materials to be used as cathodes in lithium batteries.

19.9.2 Halides-containing Melts

Fluorine is produced by electrolysis of molten salts on carbon anodes including KF–2HF at about 100°C, potassium bifluoride at about 250°C, and fluoride salts at about 1000°C. The decomposition potential of molten potassium bifluoride is 1.75 V at 250°C, a value close to that estimated thermodynamically [80]. The kinetics of the anodic process is characterized by a Tafel slope of 0.56 V per decade, $j_0 = 1 \times 10^{-4} \, A/cm^2$ [81], and by a complex reaction mechanism involving the formation of fluorine atoms on carbon. During the electrolysis, C–F surface compounds on the carbon anode are formed via side reactions. Intercalation compounds such as $(CF)_n$ contribute to the anodic effect in the electrochemical cell, which can be made less harmful by addition of LiF.

The kinetics of the chlorine electrode in different chloride melts was studied in the range 190–430°C. Different controlled processes involving the participation of chlorine atoms on graphite have been proposed [82, 83].

The evolution and dissolution of chlorine at graphite electrodes was studied in molten lithium chloride. The anodic evolution involves a fast discharge of chloride ions followed by the combination of chlorine atoms that is the rds

of the process. The graphite surface is appreciably covered by chlorine species under Temkin adsorption conditions.

The cathodic dissolution of chlorine is limited by diffusion of chlorine in the melt to the electrode surface under high current conditions, whereas at low currents the process of dissociation of chlorine on the surface is followed by the charge transfer process [83].

19.9.3 Oxygen-containing Melts

Deposition of carbon from the electrolysis of molten carbonates (Li_2CO_3, Na_2CO_3, and K_2CO_3) involves the gradual reduction of the degree of oxidation of carbonate to carbon. At temperatures below 700°C, the formation of carbon is thermodynamically favored compared to that of carbon monoxide [6].

Voltammetry data of graphite electrodes in molten $NaNO_3/KNO_3$ at 240–350°C indicate an anodic reaction involving O_2^- ion and NO that proceeds via an oxide group on the graphite surface. The corrosion of graphite was related to the formation of a NO_3 intermediate [84, 85].

For graphite in $NaNO_2/KNO_2$ melt at 236°C no appreciable corrosion was observed [86, 87].

The kinetics of the hydrogen electrode reaction on dense porous graphite electrodes in molten $KHSO_4$ from 245°C to 280°C [88–90] showed that the cathodic and anodic reactions are not strictly conjugated processes. The cathodic reaction was discussed in terms of conventional mechanisms, but the anodic reaction involves the simultaneous oxidation of hydrogen and graphite surface. The reaction exhibits a one-half power dependence on hydrogen pressure.

The kinetics of the electro-oxidation of graphite in molten $KHSO_4$ to volatile compounds (carbon dioxide, carbon monoxide, and traces of sulfur dioxide) was studied in the range 180–320°C. The faradaic yield for carbon dioxide (4 F per mol of carbon dioxide) is about 90 %. The rds is the desorption of oxygen-containing intermediate species [91].

19.10 CARBON ELECTRODE MANUFACTURING TECHNIQUES

Industrial carbon materials are used for molds, structural forms, electrodes of all kinds to be used in current production, metal deposition, and chemicals manufacturing [92]. Their fabrication involves a number of specific operations and processes. For instance, carbon blacks are deposited, collected, and processed. Cokes must be crushed and calcined; binders (pitches) must be pulverized and classified. Green mixtures are formed, molded, extruded, baked, and some carbons are also graphitized to provide special properties.

Different electrode designs were developed. Porous conductive electrodes having at least two zones can be used either as reversed dual porosity electrode or as electrode assembly with conductive, noncompressible porous carbon matrices [92].

The gas–diffusion electrode constitutes a system in which a reactive gas is supplied under pressure to a porous electrode partition that separates gas and electrolyte phases from each other [93]. By adjusting the gas pressure and average pore diameter, the electrolyte fills only part of the pore chemical system.

In recent years, the preparation and properties of Pt–Ru/C electrocatalysts for polymer electrolyte fuel cell applications have received considerable attention [94–97].

ACKNOWLEDGMENTS

REFERENCES

1. Parsons, R. (1959). *Equilibrium Properties of Electrified Interfaces, Modern Aspects of Electrochemistry*, Vol. 1. Butterworth.
2. Conway, B.E. (1965). *Theory and Principles of Electrode Processes.* Ronald Press Co.
3. Pourbaix, M. (1966). *Atlas of Electrochemical Equilibria in Aqueous Solutions.* Pergamon Press.
4. de Bethune, A.J. and Swendeman Loud, N.A. (1964). *The Encyclopedia of Electrochemistry.* Reinhold, p. 414.
5. Charlot, G., Bézier, D., and Courtot J. (1958). *Tables of Constants and Numerical Data*, Vol. 8. Pergamon.
6. Randin, J.-P. (1976). *Encyclopedia of Electrochemistry of the Elements*, Vol. VII. Marcel Dekker, Chapter VII-1.
7. Pourbaix, M. (1970). Rapport Technique CEBELCOR, 115, RT 181-182; Science et Technique, No. 7/7, 9/10, 11/12 (1947) and 1/2 (1948).
8. Pourbaix, M. (1973). *Lectures on Electrochemical Corrosion.* Plenum Press.
9. Delimarskii, I.K. and Markov, B.F. (1961). *Electrochemistry of Fused Salts.* The Sigma Press.
10. Alabyshev, A.F., Lantratov, M.F., and Morachevskii, A.G. (1965). *Reference Electrodes for Fused Salts.* Press Publishers, p. 112.
11. Creighton, H.J. (1951). *Principles and Applications of Electrochemistry*, Vol. I. John Wiley & Sons.

12. Beck, F. (1997). *Graphite, Carbonaceous Materials and Organic Solids as Active Electrodes in Metal-Free Batteries, Advances in Electrochemical Science and Engineering*, Vol. 5. Wiley-VCH.
13. Kinoshita, K. (1988). *Carbon: Electrochemical and Physicochemical Properties*. Wiley.
14. Weinberg, N.L. (1982). *Techniques of Electro-Organic Synthesis*, Vol. 1–3.
15. Baizer, M. and Lund, H. (1985). *Organic Electrochemistry*. Marcel Dekker.
16. Conway, B.E. (1999). *Electrochemical Supercapacitors*. Kluwer Academic Plenum Publishers.
17. Dresselhaus, G. (1984). Electronic and lattice properties of graphite. *Proceedings of the Workshop on the Electrochemistry of Carbon*. Pennington: The Electrochemical Society, p. 5.
18. Dresselhaus, M.S., Dresselhaus, G., and Saito, R. (1999). Nanotechnology in carbon materials. In *Nanotechnology* (G.L. Timp, ed.). Springer, Chapter 7.
19. Saito, R., Dresselhaus, G., and Dresselhaus M.S. (1996). Tunneling conductance of connected carbon nanotubes. *Phys. Rev. B*, **53**, 2044–50.
20. McCreery, R.C. (1991). Structural effects of carbon electrodes. *Electroanalytical Chemistry*, Vol. 17. Marcel Dekker.
21. Thrower, P.A. (1982). Microstructures of carbon materials. *Proceedings of the Workshop on the Electrochemistry of Carbons*, Vol. 84–5. Pennington: The Electrochemical Society, p. 40.
22. Lamb, A.B. and Elder, L.W. (1931). The electromotive activation of oxygen. *J. Am. Chem. Soc.*, **53**, 137–63.
23. Singer, L.S. (1982). Electron paramagnetic resonance (EPR) in carbons. *Proceedings of the Workshop on the Electrochemistry of Carbons*, Vol. 84–5. Pennington: The Electrochemical Society, p. 26.
24. Golden, T.C., Jenkins, R.G., Otake, Y., and Scaroni, A.W. (1982). Oxygen complexes on carbon materials. *Proceedings of the Workshop on the Electrochemistry of Carbons*, Vol. 84–5. Pennington: The Electrochemical Society, p. 61.
25. Studebaker, M.L., Hoffman, E.W.D., Wolfe, A.C., and Nabors L.G. (1956). Oxygen containing groups on the surface of carbon black. *Ind. Eng. Chem.*, **48**, 162–6.
26. Randin, J.P. and Yeager, E. (1972). Differential capacitance study on the basal plane of stress-annealed pyrolytic graphite. *J. Electroanal. Chem.*, **36**, 257–76.
27. Morcos, I. and Yeager, E. (1970). Kinetic studies of the oxygen peroxide couple on pyrolytic graphite. *Electrochim. Acta*, **15**, 953–1.
28. Yeager, E. Molla, J.A., and Gupta, S. (1982). The electrochemical properties of graphite and carbon. *Proceedings of the Workshop on the Electrochemistry of Carbons*, Vol. 84–5. Pennington: The Electrochemical Society, p. 123.
29. Fabish, F.J. and Schleifer, D.E. (1982). Surface chemistry and the carbon black work function. *Proceedings of the Workshop on the Electrochemistry of Carbons*, Vol. 84–5. Pennington: The Electrochemical Society, p. 79.
30. Aleksandrov Yu.I. and Mashovets, V.P. (1966). Wettability of the graphite electrode in molten chlorides. *Zh. Prikl. Khim.*, **39**, 2591–6.
31. Bukun, N.G. and Tkacheva, N.S. (1969). Double-layer capacitance of a graphite electrode in molten chlorides. *Elektrokhimiya*, **5**, 596–8.
32. Ukshe, E.A. and Leonova, L.S. (1970). Chlorine diffusion in fused lithium chloride, *Elektrokhimiya*, **6**, 1423–5.
33. Thonstadt, J. (1970). The electrode reaction on the C, CO_2 electrode in cryolite-alumina melts. II. Impedance measurements. *Electrochim. Acta*, **15**, 1581–95.

34. Thonstadt, J. (1973). Double-layer capacity of graphite in cryolite–alumnina melts and surface area changes by electrolyte consumption of graphite and baked carbon. *J. Appl. Electrochem.*, **2**, 315–19.

35. Gewirth, A.A. and Bard, A.J. (1988). In situ scanning tunneling microscopy of the anodic oxidation of highly oriented pyrolytic graphite surfaces. *J. Phys. Chem.*, **92**, 55663–6.

36. Bunde, A. and Havlin, S. (1996). *Fractals and Disordered Systems*. Springer.

37. Bard, A.J. and Faulkner, L.R. (1980). *Electrochemical Methods*. John Wiley & Sons.

38. Pyun, S.I. and Rhee, C.K. (2004) An investigation of fractal characteristics of mesoporous carbon electrodes with various pore structures. *Electrochim. Acta*, **49**, 4171–80.

39. Ebert, L.B. (1982). Electrochemistry of intercalation compounds of graphite. *Proceedings of the Workshop on the Electrochemistry of Carbons*, Vol. 84–5. Pennington: The Electrochemical Society, p. 595.

40. Murray, F. (1999). Modified electrodes. *Electroanalytical Chemistry*, Vol. 13. Marcel Dekker.

41. Zagal, J. Sen, R.K., and Yeager, E. (1977). Oxygen reduction by Co(II) tetrasulfonatephthalocyanine irreversibly adsorbed on a stress-annealed pyrolytic graphite electrode surface. *J. Electroanal. Chem.*, **83**, 207–13.

42. Brown, A.P. and Anson, F.C. (1977). Molecular anchors for the attachment of metal complexes to graphite electrode surfaces. *J. Electroanal. Chem.*, **83**, 203–7.

43. Schreurs, J. and Barendrecht, E. (1984). Surface-modified electrodes. *Recl. Trav. Chim. Pays-Bas*, **103**, 205–19.

44. Dryhurst, G. (1977). *Electrochemistry of Biological Molecules*. Academic Press.

45. Matsue, T. Fujihira, M., and Osa, T. (1979). Selective chlorination with a cyclodextrin modified electrode. *J. Electrochem. Soc.*, **126**, 500–1.

46. Tarasevich, M.R., Yaropolov, A.I., Bogdanoskaya, V.A., and Varfolomeev S.D. (1979). Electrocatalysis of a cathodic oxygen reduction by laccase. *J. Electroanal. Chem.*, **104**, 393–403.

47. Yamaguchi, N.O., Nishiki, Y., Tokuda, K., and Matsuda, H. (1982). Apparent diffusion coefficients for electroactive anions in coatings of protonated poly(4-vinylpiridine) on graphite electrodes. *J. Electroanal. Chem.*, **139**, 371–82.

48. Wightman, R.M., Kovach, P.M., Kuhr, W.G., and Stutts, K.J. (1982). Increasing electrochemical reversibility at carbon electrodes. *Proceedings of the Workshop on the Electrochemistry of Carbons*, Vol. 84–5. Pennington: The Electrochemical Society, p. 510.

49. McLean, J.D. (1982). Carbon electrodes for liquid chromatography detection. *Anal. Chem.*, **54**, 1169–74.

50. Anderson, J.E. Hopkins, D. Shadrick, J.W., and Ren Y. (1989). Apparatus for the fabrication of poly(chlorotrifluoroethylene) composite electrodes. *Anal. Chem.*, **61**, 2330–2.

51. Park, J. and Shaw, B.R. (1989). Electrochemical performance of crosslinked poly(styrene)-co-poly(vinylpyridine) composite electrodes containing carbon blacks. *Anal. Chem.*, **61**, 848–52.

52. Falat, L. and Cheng, H.Y. (1983). Electrocatalysis of ascorbate and NADH at a surface modified graphite epoxy electrode. *J. Electroanal. Chem.*, **157**, 393–7.

53. de Bettencourt-Dias, A., Winkler, K., Fawcett, W.R., and Balch, A.L. (2003). The influence of electroactive solutes on the properties of electrochemically formed fullerene C_{60}-based films. *J. Electroanal. Chem.*, **549**, 109–17.

54. Tan, W.T., Bond, A.M., Ngooi, S.W., et al. (2003). Electrochemical oxidation of L-cysteine mediated by a fullerene-C_{60}-modified carbon electrode. *Anal. Chim. Acta*, **491**, 181–91.
55. Levich, B.G. (1962). *Physicochemical Hydrodynamics*. Prentice-Hall.
56. Albery, W.J. and Hitchmann, M.I. (1971). *Ring-Disc Electrodes*. Clarendon Press.
57. Zagal, J., Bindra, P., and Yeager, E. (1980). A mechanistic study of oxygen reduction on water soluble phtalocyanine adsorbed on graphite electrodes. *J. Electrochem. Soc.*, **127**, 1506–17.
58. Collman, J.P., Denisevich, P., Konai, K., et al. (1980). Electrode catalysis of the four-electron reduction of oxygen to water by dicobalt face-to-face porphyrins. *J. Am. Chem. Soc.*, **102**, 6027–36.
59. Damjanovic, A., Genshaw, M.A., and Bockris, J.O'M. (1967). The role of hydrogen peroxide in oxygen reduction at platinum in H_2SO_4 solution. *J. Electrochem. Soc.*, **114**, 466–72.
60. Lu, J.T., Tryk, D., and Yeager, E. (1982). Determination of the equilibrium constant for the superoxide dismutation. Extended Abstracts of the Electrochemical Society Meeting, Abstract 82-1.
61. Gimeno, Y., Hernández Creus, A., González, S., et al. (2001). Preparation of 100–160 nm sized branched Pd islands with enhanced electrocatalytic properties in HOPG. *Chem. Mater.*, **13**, 1857–64.
62. Gimeno, Y., Hernández Creus, A., Carro, P., et al. (2002). Electrochemical formation of Pd islands on HOPG: kinetics, morphology and growth mechanism. *J. Phys. Chem. B*, **106**, 4232–44.
63. Boxley, Ch., J., White, H.S., Listex, T.E., and Pinhero, P.J. (2003). Electrochemical deposition and reoxidation of Au at HOPG. Stabilisation of Au nanoparticles on the upper plane of step edges. *J. Phys. Chem. B*, **107**, 451–8.
64. Liu, H.Y., Weaver, M.J., Wang, C.B., and Chang C.K. (1983). Dependence of electrocatalysis for oxygen reduction by adsorbed dicobalt cofacial porphyrins upon catalyst structure. *J. Electroanal. Chem.*, **145**, 439–47.
65. Iliev, I. (1981). Air cathodes for primary metal air batteries. Extended Abstracts of the Electrochemical Society National Meeting.
66. Salimi, A., Banks, C.E., and Compton, R.G. (2003). Ultrasonic effects on the electroreduction of oxygen at a glassy carbon anthraquinone-modified electrode. The Koutecky-Levich equation applied to insonated electrocatalytic reactions. *Phys. Chem. Chem. Phys.*, **5**, 3988–93.
67. Szücs, A., Budavári, V., Berkesi, O., and Novak M. (2003). Electrochemical hydrogenation of C_{60} fullerene films. *J. Electroanal. Chem.*, **548**, 131–7.
68. Tarasevich, M.R. and Khrushcheva, E.I. (1989). *Electrocatalytic Properties of Carbon Materials, Modern Aspects of Electrochemistry*, Vol. 19. Plenum Press, p. 205.
69. Janssen, L.J. and Hoogland, J.G. (1970). The electrolysis of an acidic NaCl solution with a graphite anode. III. Mechanism of chlorine evolution. *Electrochim. Acta*, **15**, 941–51.
70. Fang, C. and Zhon, Y. (2001). The electrochemical characteristics of C_{60}-glutathione modified Au electrode and the electrocatalytic oxidation of NADH, *Electroanalysis*, **13**, 949–54.
71. Chen, T., Barton, S., Binyamin, G., et al. (2001). A miniature biofuel cell. *J. Am. Chem. Soc.*, **123**, 8630–1.
72. Mano, N., Mao, F., and Heller, A. (2002). A miniature biofuel cell operating in a physiological buffer. *J. Am. Chem. Soc.*, **124**, 12962–5.

73. Stonehart, P. and MacDonald, J.P. (1982). Corrosion of carbons in acid electrolytes. *Proceedings of the Workshop on the Electrochemistry of Carbons*, Vol. 84–5. Pennington: The Electrochemical Society, p. 292.

74. Kokhenov, G. and Milova, N. (1969). Effect of pH on the anodic oxidation of graphite. *Elektrokhimiya*, **5**, 93–6.

75. Kinoshita, K. and Bett, J. (1973). Electrochemical oxidation of carbon black in concentrated phosphoric acid at 135C. *Carbon*, **11**, 237.

76. Kinoshita, K. and Bett, J.A.S. (1974). Corrosion problems in energy conversion and generation. *The Electrochemical Society*.

77. Koehler, W.A. (1951). *Principles and Applications of Electrochemistry*, Vol. II. John Wiley & Sons.

78. Galloni, P. (1973). *Trattato di Ingenieria Eletrochimica*. Tamburini.

79. Thonstadt, J. (1970). The electrode reaction on the C, CO_2 electrode in cryolite-alumina melts. I. Steady state measurements. *Electrochim. Acta*, **15** 1569–80.

80. Arvia, A.J. and de Cusminsky, J.B. (1967). El Potencial del Electrodo de Flúor en el Bifluoruro de Potasio Fundido. *An. Asoc. Quim. Arg.*, **55**, 41–6.

81. Arvia, A.J. and de Cusminsky, J.B. (1962). Kinetics of the electrochemical formation of fluorine at carbon electrodes. *Trans. Faraday Soc.*, **58**, 1019–32.

82. Vandenbroele, H.J. and Arvia, A.J. (1967). Estudio Cinético del Electrodo de Cloro en Medios Iónicos Fundidos. *An. Asoc. Quim. Arg.*, **55**, 21–40.

83. Triaca, W.E. Solomons, C., and Bockris, J.O.M. (1968). The mechanism of the electrolytic evolution and dissolution of chlorine on graphite. *Electrochim. Acta*, **13**, 1949–64.

84. Arvia, A.J. and Triaca, W.E. (1965). Anodic reactions of molten nitrates on graphite. *Electrochim. Acta*, **10**, 1188–9.

85. Arvia, A.J. and Triaca, W.E. (1966). Electrolysis of molten nitrates on graphite electrodes: kinetics of the anodic reaction. *Electrochim. Acta*, **11**, 975–88.

86. Arvia, A.J. and Calandra, A.J. (1967). Kinetics of the discharge of nitrite ions in the electrolysis of molten nitrites on graphite electrodes. *Electrochim. Acta*, **12**, 1441–55.

87. Sustersic, M.G. Triaca, W.E., and Arvia, A.J. (1974). Potentiodynamic behaviour of graphite and platinum electrodes in sodium nitrite-potassium nitrite melts. *Electrochim. Acta*, **19**, 19–25.

88. Balskus, E.J., Podestá, J.J., and Arvia, A.J. (1970). Kinetics of electrochemical hydrogen evolution and dissolution on graphite in molten $KHSO_4$. *Electrochim. Acta*, **15**, 1557–8.

89. Balskus, E.J., Podestá, J.J., and Arvia, A.J. (1971). Hydrogen evolution and dissolution on graphite electrodes in the electrolysis of molten $KHSO_4$. I. Kinetics of the reactions on dense graphite. *Electrochim. Acta*, **16**, 1663–70.

90. Balskus, E.J., Triaca, W.E., and Arvia, A.J. (1972). Hydrogen evolution and dissolution on graphite electrodes in molten potassium bisulphate. II. Kinetics and mechanism of the reactions on porous graphite. *Electrochim. Acta*, **17**, 45–62.

91. Arvia, A.J., Triaca, W.E., and Videla, A.H. (1970). Kinetics and mechanism of the electrochemical oxidation of graphite in bisulphate melts. *Electrochim. Acta*, **15**, 9–24.

92. Kordesch, K., Jahangir, S., and Schautz, M. (1982). Carbon electrodes manufacturing techniques. *Proceedings of the Workshop on the Electrochemistry of Carbons*, Vol. 84–5. Pennington: The Electrochemical Society, p. 387.

93. Bockris, J.O'M. and Srinivasan, S. (1969). *Fuel Cells: Their Electrochemistry*. McGraw-Hill.

94. Schneider, J., Wambach, C., Pennemann, B., and Wandelt, K. (1999). Scanning tunneling microscopy and scanning tunneling spectroscopy studies of powdery palladium/graphite model catalysts. *Langmuir*, **15**, 5765–72.
95. Pozzio, A., Silva, R.F., De Francesco, M., et al. (2002). A novel route to prepare stable PtRu/C electrocatalysts for polymer electrolyte fuel cell. *Electrochim. Acta*, **48**, 255–62.
96. Steigerwalt, E.S., Deluga, G.A., Cliffel, D.E., and Lukehart, C.M. (2001). A Pt-Ru/graphitic carbon nanofiber nanocomposite exhibiting high relative performance as a direct-methanol fuel cell anode catalyst. *J. Phys. Chem. B*, **105**, 8097–101.
97. Adora, S., Soldo-Olivier, Y., Fauré, R., et al. (2001). Electrochemical preparation of platinum nanocrystallites on activated carbon studied by X-ray absorption spectroscopy. *J. Phys. Chem. B*, **105**, 10489–95.